Energy relaxation dynamics in a nodal-line semimetal

Benjamin M. Fregoso ⬤,[1] Madhab Neupane,[2] and Anup Pradhan Sakhya[2]

[1]*Department of Physics, Kent State University, Kent, Ohio 44242, USA*
[2]*Department of Physics, University of Central Florida, Orlando, Florida 32816, USA*

We study the temperature relaxation dynamics of nodal-line semimetals after a sudden excitation in the presence of acoustic and optical phonon modes. We find that the nodal line constrains the electron momenta in scattering processes, and as a result, the temperature relaxation due to acoustic phonons is exponential as a function of time. However, depending on initial conditions, other functional forms are possible. In typical pump-probe experiments, the temperature relaxation is linear due to acoustic phonons with rates that vary as $\sim n^{1/2}$ with density. The temperature relaxation due to optical phonons is also linear with rates $\sim n^{-1/2}$ or $\sim n$.

I. INTRODUCTION

Energy dissipation via phonon scattering is the main pathway to thermalization in electronic systems [1–5]. Energy relaxation in metals has been extensively studied in the context of pump-probe experiments where electrons are excited via short laser pulses. After the initial excitation, electrons lose energy to the lattice degrees of freedom and eventually reach equilibrium.

In a typical pump-probe experiment, the temperature initially falls rapidly due to optical phonon emission. Below a certain crossover temperature, optical phonon emission becomes less efficient, and a slower decay associated with acoustic phonons sets in. While this scenario is understood, the effects of the Fermi surface (FS) topology on the relaxation dynamics are just beginning to be explored. For example, it is known that at low temperature, the so-called phonon cooling power scales as $\mathcal{P} \propto T_e^\kappa - T_L^\kappa$ with the instantaneous electron temperature T_e and the lattice temperature T_L. For a conventional three-dimensional (3D) metal [1,4], $\kappa = 5$, but for thin films [6,7], $\kappa = 6$. If the phonon phase space is constrained [8], $\kappa = 3$, and for graphene [9], $\kappa = 4$.

Of recent interest is the relaxation dynamics of Dirac materials which have zero-energy manifolds embedded in the Brillouin zone [10]. For example, graphene and topological insulators are two-dimensional (2D) semimetals with zero-energy points (Dirac points). Near the Dirac point the quasiparticle dispersion is linear in momentum. As a consequence of its small FS, graphene exhibits strong suppression of electron-phonon scattering below the Bloch-Grüneisen temperature [11,12] and novel disorder-mediated electron-phonon scattering [13–15]. Graphene also exhibits $T_e \sim 1/\sqrt{t}$ temperature relaxation as a function of time due to acoustic phonon relaxation [16–18].

Weyl (or Dirac) semimetals (SMs) are different Dirac materials in that they are 3D SMs with zero-energy (Weyl) points. Near Weyl points, the FS is a sphere instead of a circle. They exhibit asymmetric Fano line shapes [19] and a strong electron-phonon coupling constant [20]. The temperature relaxation in Weyl SMs varies as $T_e \sim 1/\sqrt[3]{t}$ (at long times) due to acoustic phonon scattering [21].

The discovery of nodal-line semimetals (NLSMs) [22,23] added another member to the family of Dirac materials. NLSMs are 3D semimetals with zero-energy *lines* in momentum space. NLSMs can also be classified by topological invariants [23–25] and were demonstrated experimentally in PbTaSe$_2$ [26], PtSn$_4$ [27], and ZrSiS [28,29] with other materials being investigated [30,31]. NLSMs exhibit unusual magnetoresistance [32], strong light-matter interactions [33], and correlation-induced reduction of free carrier Drude weight [34]. They are predicted to exhibit a quasi-topological electromagnetic response [35], enhanced excitonic instability [36], low Coulomb screening [37], and diverging mobility [38].

In this paper, we investigate the temperature relaxation dynamics of NLSMs and, in particular, the role of the nodal line. We find that despite the complex FS topology of NLSMs the relaxation due to acoustic phonons is exponential, just as in typical 3D metals. In a NLSM, phonon scattering events constrain the electron's initial and final momenta to be close to the nodal line. This has two important consequences: (a) at high temperatures the acoustic phonon cooling power is

TABLE I. Temperature scaling of the cooling power $\mathcal{P}_a$ and the heat capacity $\mathcal{C}$ for NLSMs, graphene, and Weyl SMs. $\mathcal{C}$ is sensitive to the volume of the FS, whereas $\mathcal{P}_a$ is sensitive to the topology of the FS. NLSMs have small $\mathcal{P}_a$ and small $\mathcal{C}$, which result in exponential temperature relaxation. Graphene and Weyl SMs, on the other hand, have slower $1/\sqrt{t}$ and $1/\sqrt[3]{t}$ temperature relaxations, [see Eq. (1)].

	NLSM	Graphene	Weyl
Spatial dimension	3	2	3
Nodal dimension	1	0	0
$\mathcal{C} \sim T_e^c$, $c =$	2	2	3
$\mathcal{P}_a \sim T_e^p$, $p =$	3	5	7
$\mathcal{P}_a/\mathcal{C} \sim T_e^{p-c}$	1	3[a]	4[b]

[a]Reference [16].
[b]Reference [21].

TABLE II. Electron temperature as a function of time in NLSMs, graphene, and Weyl SMs for various limits. T_e is the electron temperature, ω_0 is the optical phonon energy, μ is the chemical potential, T_L is the lattice temperature, exp indicates exponential, lin indicates linear, and inv log indicates the inverse log. By low density we mean $\mu \ll k_B T_e$ and by high density $\mu \gg k_B T_e$. Only the tails of the relaxation functions are shown. The reference indicates the relevant equation in the text. For clarity we omit $\hbar$ and k_B.

	NLSM	Weyl SM	Graphene
Spatial dimension	3	3	2
Nodal dimension	1	0	0
	Optical phonon relaxation		
Low density: $\omega_0 \gg T_e \gg T_L, \mu$	inv log, (20)	inv log, (D6)	inv log, (20)
Low density: $T_e \gg \omega_0, T_L, \mu$	exp, (22)	$1/t$, (D7)	exp, (22)
High density: $\mu, \omega_0 \gg T_e \gg T_L$	inv log, (27)	inv log, (D11)	inv log, (27)
High density: $\mu \gg T_e \gg \omega_0, T_L$	lin, (29)	lin, (D14)	lin, (29)
	Acoustic phonon relaxation		
Low density: $T_e \gg T_L, \mu$	exp, (32)	$1/\sqrt[3]{t}$, (D19) [21]	$1/\sqrt{t}$, (E5) [16]
Low density: $T_e \gtrsim T_L, (\mu = 0)$	exp, (32)	exp, (D19) [21]	exp, (E5) [16]
High density: $\mu \gg T_e \gg T_L$	lin, (33)	lin, (D21) [21]	lin, (E6) [16]
High density: $\mu \gg T_e \gtrsim T_L$	exp, (33)	exp, (D21) [21]	exp, (E6) [16]

much lower than that of Weyl SMs or graphene (see Fig. 5 below), and (b) at low temperatures it gives the exponential temperature relaxation, which is different from a power-law relaxation obtained in Weyl SMs and graphene. To understand this, we write the relaxation equation as

$$\frac{dT_e}{dt} \sim -\frac{\mathcal{P}_a}{\mathcal{C}} \sim -T_e^{p-c}, \qquad (1)$$

where $\mathcal{C} = d\mathcal{E}/dT_e$ is the heat capacity and $\mathcal{P}_a$ is the phonon cooling power. As can be seen from Table I, $p - c = 1$ for NLSMs, $p - c = 3$ for graphene, and $p - c = 4$ for Weyl SMs.

In a typical pump-probe experiment with an initial temperature $T_0 \sim 100$ meV, Fermi level $\epsilon_F \sim 300$ meV, and optical modes around $\hbar\omega_0 \sim 30$ meV, the predicted relaxation is linear in both the acoustic and optical phonon regimes (see Table II). The density dependence is different in each case (see Secs. III and IV). In fact, linear temperature relaxation is common to all Dirac materials in this regime. To obtain these results we use a simple two-band model consisting of a ring (nodal line) in momentum space [23]. Our main assumptions are: (a) the electrons are in equilibrium among themselves at temperature T_e, (b) the phonons are in equilibrium among themselves at a fixed temperature T_L, and (c) the temperature is higher than the Bloch-Grüneisen temperature.

This paper is organized as follows. We first consider optical and acoustic phonon branches separately, obtaining analytic solutions in various limits (Secs. II, III, and IV). The solutions are then used to give expressions for the crossover temperature between the optical- and acoustic-phonon regimes in Sec. V. In Sec. VI we give numerical solutions including both phonon branches. A simple scaling argument is given in Sec. VII to intuitively understand temperature relaxation due to acoustic phonons, and we conclude in Sec. VIII. The Appendixes include some calculation details.

II. PHONON COOLING POWER

A simple mathematical model of the electron's energy loss is

$$\frac{d\mathcal{E}}{dt} = -\mathcal{P}, \qquad (2)$$

where $\mathcal{E}(t)$ is the energy of the ensemble assumed to depend on temperature and chemical potential $\mathcal{E}(t) = \mathcal{E}(\mu(t), T_e(t))$ and $\mathcal{P}$ is the rate of energy transfer from the electrons to the lattice, i.e., cooling power [1],

$$\mathcal{E} = \frac{1}{V} \sum_{n\mathbf{k}} \epsilon_{n\mathbf{k}} f_{n\mathbf{k}}, \qquad (3)$$

$$\mathcal{P} = \frac{1}{V} \sum_{n\mathbf{k}} \epsilon_{n\mathbf{k}} \frac{df_{n\mathbf{k}}}{dt}. \qquad (4)$$

Importantly, $\mathcal{P}$ depends on $\mu(t)$ and $T_e(t)$ via the collision integral. $\epsilon_{n\mathbf{k}}$ is the quasiparticle energy. This hydrodynamic approach [39,40] assumes that the chemical potential and temperature are well defined at all times, a reasonable assumption if electron-electron interactions thermalize the electron ensemble much faster than phonons. The collision integral for phonon scattering is

$$\frac{df_{n\mathbf{k}}}{dt} = \sum_{m\mathbf{p}} [f_{n\mathbf{k}}(1 - f_{m\mathbf{p}})W_{n\mathbf{k},m\mathbf{p}} - (n\mathbf{k} \leftrightarrow m\mathbf{p})], \qquad (5)$$

with scattering rate

$$W_{n\mathbf{k},m\mathbf{p}} = \frac{2\pi}{\hbar} \sum_{\mathbf{q}} M_{\mathbf{q}} [(N_L+1)\delta_{\mathbf{k},\mathbf{p}+\mathbf{q}} \delta(\epsilon_{n\mathbf{k}} - \epsilon_{m\mathbf{p}} - \hbar\omega_{\mathbf{q}})$$
$$+ N_L \delta_{\mathbf{k},\mathbf{p}-\mathbf{q}} \delta(\epsilon_{n\mathbf{k}} - \epsilon_{m\mathbf{p}} + \hbar\omega_{\mathbf{q}})]. \qquad (6)$$

Here $f_{n\mathbf{k}} \equiv f(\epsilon_{n\mathbf{k}}) = [e^{(\epsilon_{n\mathbf{k}} - \mu)/k_B T_e} + 1]^{-1}$ is the Fermi distribution function, $N_L \equiv N_L(\hbar\omega_{\mathbf{q}}) = [e^{\hbar\omega_{\mathbf{q}}/k_B T_L} - 1]^{-1}$ is the Bose distribution function evaluated at the lattice temperature T_L, T_e is the electron temperature, $M_{\mathbf{q}} = \hbar^2 D^2 q^2 (1 + s_{nm}\cos\theta)/4\rho V \hbar\omega_{\mathbf{q}}$ is the amplitude of electron-phonon scattering, $\mathbf{q}$ is the phonon momentum, $\omega_{\mathbf{q}}$ is the phonon dispersion relation, D is the deformation potential of acoustic phonons, ρ is the ion mass density, V is the volume, θ is the angle between $\mathbf{k}$ and $\mathbf{p}$, and $s_{nm} = 1(-1)$ is intraband (interband) scattering. The quasiparticle dispersion of the NLSM near the ring is

$$\epsilon_{n\mathbf{k}} = nv\hbar[k_z^2 + (k - Q)^2]^{1/2}, \qquad (7)$$

where $n = 1 (-1)$ denotes the conduction (valence) band, v is the velocity of nodal quasiparticles, and Q is the radius of
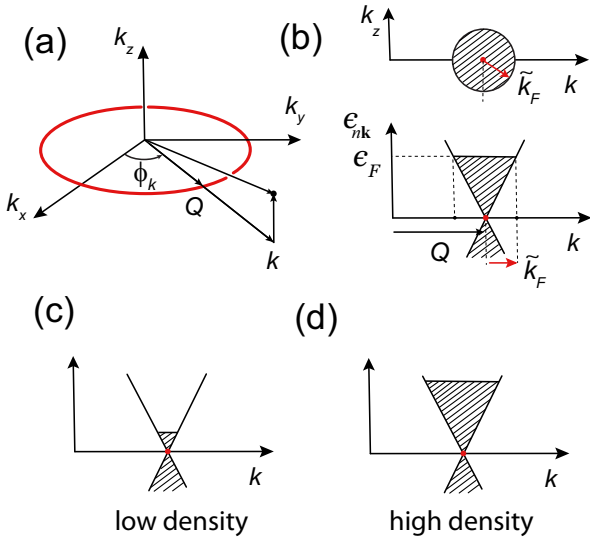
FIG. 1. (a) Nodal line (red ring) in a nodal-line semimetal (NLSM) model. (b) Quasiparticles have linear dispersion near points $(k, \phi_\mathbf{k}, k_z) = (Q, \phi_\mathbf{k}, 0)$, $0 \leqslant \phi_\mathbf{k} < 2\pi$. In the plane k-k_z the states within radius $\tilde{k}_F$ are occupied, and the Fermi surface is a torus in momentum space. (c) and (d) Two limiting cases considered analytically. The low-density regime is defined by $\mu \ll k_B T_e$, and the high-density regime is defined by $\mu \gg k_B T_e$.

the nodal ring [see Fig. 1(a)]. We consider spinless fermions. From Eqs. (5) and (6), we write Eq. (4) as [16,17]

$$\mathcal{P} = \frac{2\pi}{V} \sum_{n\mathbf{k}m\mathbf{p}} \omega_\mathbf{q}(f_{n\mathbf{k}} - f_{m\mathbf{p}})(N_L - N_e)M_\mathbf{q}$$

$$\times \, \delta(\epsilon_{n\mathbf{k}} - \epsilon_{m\mathbf{p}} - \hbar\omega_\mathbf{q}), \tag{8}$$

(see also Appendix A). We define $\mathbf{q} = \mathbf{p} - \mathbf{k}$. We assume Eq. (5) does not vanish even when we have equilibrium distributions of bosons and fermions. The nonvanishing equation (8) for $T_e \neq T_L$ is consistent with this assumption [3]. The radius of the nodal line Q is assumed to be the largest momentum scale in the system, i.e., $Q \gg |k_F - Q|, k_B T_e/v\hbar, \omega_0/v$. We also assume phonons with momenta $2Q$ are always thermally excited. This requires a minimum temperature, the Bloch-Grüneisen temperature T_{BG}; that is, we require $k_B T_e > k_B T_{\mathrm{BG}} = \hbar c 2Q$, where c is the speed of sound.

III. OPTICAL PHONON RELAXATION

In this section, we analytically calculate the temperature relaxation of a NLSM due to optical phonons. We consider a single optical phonon branch with constant energy dispersion $\omega_\mathbf{q} = \omega_0$ and constant electron-phonon matrix element $M_\mathbf{q} \equiv g^2/V$. From Eq. (8), we obtain

$$\frac{d\mathcal{E}}{dt} = -\mathcal{P}_o, \tag{9}$$

where

$$\mathcal{P}_o = \frac{g^2 Q^2 \omega_0^4}{2\pi v^4 \hbar} F(\mu, T_e)(N_e - N_L) \tag{10}$$

$$F(\mu, T_e) \equiv \int_{-\infty}^{\infty} dx |x(x-1)|[f(\hbar\omega_0 x - \hbar\omega_0) - f(\hbar\omega_0 x)]. \tag{11}$$

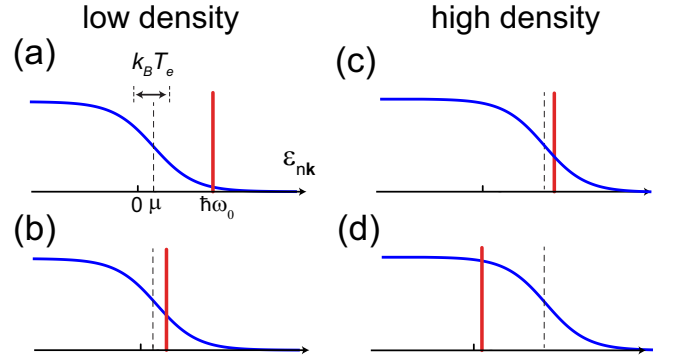$N_e = N_e(\hbar\omega_0)$, and $N_L = N_L(\hbar\omega_0)$ (see Appendix B). As seen from the factor in parentheses in Eq. (10), $\mathcal{P}_0$ is exponentially suppressed at temperatures $k_B T_e \ll \hbar\omega_0$, and hence, in this regime, we expect acoustic phonon scattering to dominate. The energy is a function of μ (assumed to be positive) and T_e, which, in turn, are functionally related due to the constant-density condition. In our NLSM model the energy and electron density are

$$\mathcal{E} = \frac{1}{V} \sum_{n\mathbf{k}} \epsilon_{n\mathbf{k}} f_{n\mathbf{k}} = \frac{v\hbar Q}{2\pi} I_{2+}, \tag{12}$$

$$n = \frac{1}{V} \sum_{n\mathbf{k}} f_{n\mathbf{k}} = \frac{Q}{2\pi} I_{1-}, \tag{13}$$

where

$$I_{n\pm} \equiv \int_0^\infty \tilde{k}^n d\tilde{k} \, [f_{c\tilde{k}} \pm (1 - f_{v\tilde{k}})], \tag{14}$$

$f_{n\tilde{k}} = [e^{\beta(nv\hbar\tilde{k} - \mu)} + 1]^{-1}$, and $\beta \equiv 1/k_B T_e$. The density is measured with respect to the nodal line.

A. Low-density limit

By low density we mean $\mu \ll k_B T_e$ and $\mu \gtrsim 0$; that is, the system is half filled. $k_B T_L$ is assumed to be zero or close to zero. However, the relative sizes of $k_B T_e$ and $\hbar\omega_0$ give various relaxation behaviors which we now consider in detail.

Case 1: $\hbar\omega_0 \gg k_B T_e \gg k_B T_L, \mu$. Figure 2(a) illustrates this situation. The dashed line indicates the position of μ, and the red line shows the position of $\hbar\omega_0$; 0 indicates the position of the nodal line. In this scenario, high-energy electrons at the tail of the distribution lower their energy by emitting optical phonons and dropping to unoccupied states. A rapid thermalization among electrons (not included here) creates a new Fermi distribution at lower temperature. If the energy of the optical phonon is too large, the cooling becomes

inefficient. Interestingly, the temperature at which optical phonon cooling stops is not of the order $\hbar\omega_0$ but could be an order of magnitude smaller (see Sec. V).

To begin, we note that if $\mu = 0$, Eq. (11) is a function of only $\bar{\beta} \equiv \hbar\omega_0/k_B T_e$ and can be integrated analytically in terms of polylogarithm functions. The first two terms for large $\bar{\beta}$ are

$$F(0, T_e) \sim \frac{1}{6} + \frac{6\zeta(3)}{\bar{\beta}^3} + \cdots, \quad \bar{\beta} \gg 1. \quad (15)$$

The total time derivative of the energy (3) has two contributions: one from the density $\partial\mathcal{E}/\partial\mu = 2n$ and one from the heat capacity $\partial\mathcal{E}/\partial T_e$. Now, the energy and chemical potential in the limit of low density $\mu \ll k_B T_e$ are

$$\mathcal{E} = \frac{Q k_B^3 T_e^3 3\zeta(3)}{2\pi v^2 \hbar^2} + \frac{Q k_B T_e \log(2)}{\pi v^2 \hbar^2}\mu^2 + \cdots \mu \ll k_B T_e, \quad (16)$$

$$n = \frac{Q k_B T_e \log(2)}{\pi v^2 \hbar^2}\mu + \cdots. \mu \ll k_B T_e. \quad (17)$$

From Eq. (17), we see that the contribution from the density vanishes in the limit $\mu \to 0$, and hence, Eq. (9) becomes $(\partial\mathcal{E}/\partial T_e)(\partial T_e/\partial t) = -\mathcal{P}_o$. In the variable $\bar{\beta}$, it takes the form

$$\frac{d\bar{\beta}}{dt} \sim \gamma_{on1}(\bar{\beta}^4 + 36\zeta(3)\bar{\beta} + \cdots)e^{-\bar{\beta}}, \quad (18)$$

where we assume $T_e \gg T_L$. The initial condition is $\bar{\beta}_0 = \hbar\omega_0/k_B T_0 \gg 1$ and $\gamma_{on1} = g^2 Q\omega_0/v^2\hbar^2 54\zeta(3)$. The right-hand side of Eq. (18) has a local maximum at $\bar{\beta} \sim 1$ and an exponential tail for large $\bar{\beta}$. In the limit $\bar{\beta} \gg 1$, Eq. (18) gives

$$\bar{\beta} \sim \log\left(\gamma_{on1}\bar{\beta}_0^4 t + e^{\bar{\beta}_0}\right) + 4\log\frac{T_0}{T_e} \quad (19)$$

or the inverse log

$$k_B T_e \sim \frac{\hbar\omega_0}{\log\left(\gamma_{on1}\bar{\beta}_0^4 t + e^{\bar{\beta}_0}\right)}. \quad (20)$$

In the last expression, we drop a small (for $T_e \lesssim T_0$) logarithmic correction. The relaxation timescale is $e^{\bar{\beta}_0}/\gamma_{on1}\bar{\beta}_0^4$. Note that $\bar{\beta}$ increases monotonically with time (as T_e decreases), and hence, it is enough to require $\bar{\beta}_0 \gg 1$. Figure 3(a) shows a numerical (see Sec. VI) example of optical phonon relaxation in the low-density regime (brown curve) with $\bar{\beta}_0 = 3 \gg 1$. The temperature relaxation is approximately given by Eq. (20).

Case 2: $k_B T_e \gg \hbar\omega_0, k_B T_L, \mu$. Figure 2(b) illustrates this situation. In this regime, many electrons have energy above the optical phonon mode, and hence, we expect enhanced optical phonon emission and subsequent fast relaxation. Indeed, we find an exponential relaxation in this regime. To see this, note that for $k_B T_e \gg \hbar\omega_0$ (or $\bar{\beta} \ll 1$), Eq. (11) is approximated by

$$F(0, T_e) = \frac{\pi^2}{3\bar{\beta}^2} - \frac{1}{6} + \frac{\bar{\beta}}{12} - \frac{\bar{\beta}^3}{360} + \cdots, \quad \bar{\beta} \ll 1. \quad (21)$$

If, in addition, $T_e \gg T_L$, then $N_e(\hbar\omega_0) - N_L(\hbar\omega_0) \sim k_B T_e/\hbar\omega_0 - k_B T_L/\hbar\omega_0 \sim 1/\bar{\beta}$, and to leading order the relaxation is exponential,

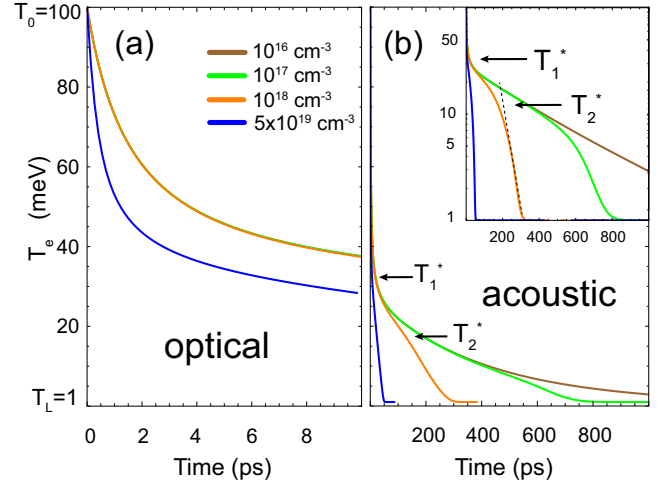$$\frac{dT_e}{dt} = -\gamma_{on2} T_e. \quad (22)$$

FIG. 3. Numerical solution for the electron temperature relaxation in a NLSM with acoustic and optical phonon modes. (a) and (b) differ only by the time resolution of the horizontal axis. Various electronic densities are considered. The initial temperature is $T_0 = 100$ meV, and the lattice temperature is $T_L = 1$ meV. The optical phonon mode is at $\hbar\omega_0 = 300$ meV, which corresponds to the regime $\hbar\omega_0 \gg k_B T_e$. The rest of the parameters are given in Table III. From (a) we see a timescale of $\tau_o = 1 - 4$ ps for optical phonon relaxation, and from (b) $\tau_a = 50 - 400$ ps, for acoustic phonon relaxation. The brown curve exhibits inverse log $\to$ exponential behaviors as T_e decreases. The orange curve exhibits inverse log $\to$ linear $\to$ exponential behaviors as T_e decreases. T_1^* is the crossover temperature separating the optical- and the acoustic-phonon regimes. T_2^* marks the transition from linear to exponential.

Here, $\gamma_{on2} = g^2 Q\omega_0\pi^2/v^2\hbar^2 27\zeta(3)$, and the relaxation timescale is $1/\gamma_{on2}$. Figure 4(a) shows the relaxation of a NLSM with the optical phonon mode energy half of the initial temperature of the electron ensemble, $\bar{\beta}_0 = 1/2$ (brown and green curves). The temperature relaxation is approximately exponential, in agreement with Eq. (22).

B. High-density limit

By high density we mean $\mu \gg k_B T_e$. Since μ is bounded from above by Fermi energy $\epsilon_F = \mu(T_e = 0)$, high density means $\epsilon_F \gg k_B T_e$. However, the relative sizes of $k_B T_e$ and $\hbar\omega_0$ give various relaxation behaviors which we now consider in detail.

Case 1: $\mu, \hbar\omega_0 \gg k_B T_e \gg k_B T_L$. Figure 2(c) illustrates this situation. To start, note that for $\mu \gg k_B T_e$, Eq. (11) becomes

$$F(\mu, T_e) \sim \left(\frac{1}{6} + \frac{2\bar{\mu}^3}{3}\right) + \frac{2\pi^2\bar{\mu}}{3\bar{\beta}^2} + \cdots, \quad \mu \gg k_B T_e, \quad (23)$$

which is obtained from the Sommerfeld expansion in variables $\bar{\mu} \equiv \mu/\hbar\omega_0$ and $\bar{\beta} \equiv \hbar\omega_0/k_B T_e$ and is valid for $\bar{\mu}\bar{\beta} \gg 1$ (or, equivalently, $\mu \gg k_B T_e$). In this limit, the energy and electron density become

$$\mathcal{E} = \frac{Q}{6\pi v^2 \hbar^2}\left(\mu^3 + \frac{\pi^2\mu}{\beta^2} + \cdots\right), \quad \mu \gg k_B T_e, \quad (24)$$

$$n = \frac{Q}{4\pi v^2 \hbar^2}\left(\mu^2 + \frac{\pi^2}{3\beta^2} + \cdots\right), \quad \mu \gg k_B T_e, \quad (25)$$
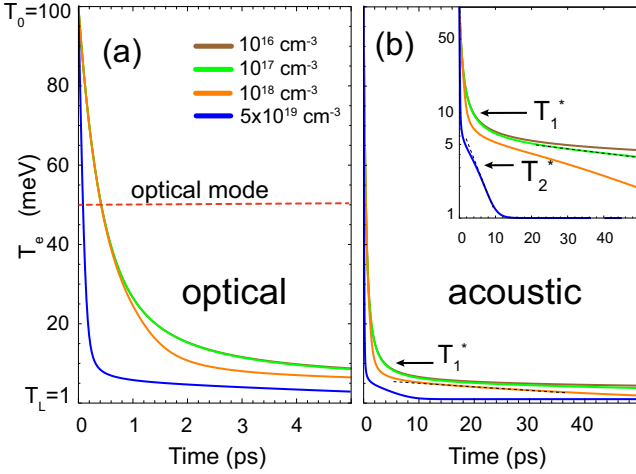
FIG. 4. Same as in Fig. 3, but with $\hbar\omega_0 = 50$ meV, i.e., $\hbar\omega_0 < k_B T_0$. The timescales are $\tau_a = 10$–50 ps and $\tau_o = 0.5$–1 ps for acoustic and optical phonon relaxations, respectively. The low density green curve exhibits transition from exponential $\rightarrow$ exponential as T_e decreases. The high density blue curve exhibits transitions linear $\rightarrow$ linear $\rightarrow$ exponential as T_e decreases.

and hence, $\mu(T_e) = \epsilon_F - \pi^2 k_B^2 T_e^2 / 6\epsilon_F + \cdots$. Also, if $\bar{\beta} \gg 1$, then $N_e - N_L \sim e^{-\hbar\omega_0/k_B T_e} - e^{-\hbar\omega_0/k_B T_L} \sim e^{-\bar{\beta}}$, and Eq. (9) becomes

$$\frac{\partial \bar{\beta}}{\partial t} = \tilde{\gamma}_{od1} \bar{\beta}^3 \left(\frac{1}{6} + \frac{2\bar{\mu}^3}{3} + \frac{2\pi^2 \bar{\mu}}{3\bar{\beta}^2} + \cdots \right) e^{-\bar{\beta}}. \quad (26)$$

Now, if $\bar{\mu}\bar{\beta} \gg \pi$, the leading behavior is an inverse log function,

$$k_B T_e = \frac{\hbar\omega_0}{\log\left(\gamma_{od1}\bar{\beta}_0^3 t + e^{\bar{\beta}_0}\right)}, \quad (27)$$

where $\gamma_{od1} = 3g^2 Q\omega_0^2(1/6 + 2\bar{\mu}^3/3)/\pi^2 v^2 \mu \hbar$. The relaxation timescale $e^{\bar{\beta}_0}/\gamma_{od1}\bar{\beta}_0^3$ is $\sim n^{1/2}$ for $\bar{\mu} \ll 1$ and $\sim n^{-1}$ for $\bar{\mu} \gg 1$; n is the electron density. Note that the timescale increases or decreases with increasing electron density. Figure 3(a) illustrates the high-density regime with parameters $\bar{\beta}_0 = 3$, $\bar{\mu} \sim \epsilon_F/\hbar\omega_0 \sim 1$ (blue curve). The relaxation is approximately given by Eq. (27).

Case 2: $\mu \gg k_B T_e \gg \hbar\omega_0, k_B T_L$. Figure 2(d) illustrates this situation. Since $\mu \gg k_B T_e$, we can use Eq. (23). In addition, if $\bar{\beta} \ll 1$ and $T_e \gg T_L$, then $N_e - N_L \sim 1/\bar{\beta}$, and Eq. (9) becomes

$$\frac{d\bar{\beta}}{dt} = \tilde{\gamma}_{od2} \bar{\beta}^2 \left(\frac{1}{6} + \frac{2\bar{\mu}^3}{3} + \frac{2\pi^2 \bar{\mu}}{3\bar{\beta}^2} \cdots \right). \quad (28)$$

Now, if $\bar{\mu}\bar{\beta} \gg \pi$, the leading behavior is linear,

$$k_B T_e = k_B T_0 - \hbar\omega_0 \gamma_{od2} t, \quad (29)$$

where $\gamma_{od2} = 3g^2 Q\omega_0^2(1/6 + 2\bar{\mu}^3/3)/\pi^2 v^2 \hbar \mu$ is $\sim n^{-1/2}$ for $\bar{\mu} \ll 1$ and $\sim n$ for $\bar{\mu} \gg 1$. The rate can increase or decrease with increasing electron density. Figure 4(a) illustrates the high-density regime with parameters $\bar{\beta}_0 = 1/2$ (blue or orange curve). The relaxation is approximately linear for temperatures above ~ 40 meV.

IV. ACOUSTIC PHONON RELAXATION

We now calculate the temperature relaxation due to acoustic phonons in the low- and high-density regimes. To obtain analytical expressions, we evaluate Eq. (8) to lowest order in $c/v \ll 1$, where c is the speed of sound, assumed to be isotropic. In this limit, acoustic phonon scattering is quasielastic, and we obtain (see Appendix C)

$$\frac{d\mathcal{E}}{dt} = -\mathcal{P}_a, \quad (30)$$

where

$$\mathcal{P}_a = \frac{D^2 Q^4 k_B}{4\pi \rho v^2 \hbar} I_{1+}(T_e - T_L). \quad (31)$$

A. Low-density limit

Setting $\mu = 0$ and using Eqs. (16), (17), and (31), we obtain

$$\frac{dT_e}{dt} = -\gamma_{an}(T_e - T_L), \quad (32)$$

where $\gamma_{an} = \pi^2 D^2 Q^3 / \rho v^2 \hbar 108 \zeta(3)$. Hence, the temperature relaxes exponentially with timescale $1/\gamma_{an}$. This should be compared with the slower $\sim 1/\sqrt{t}$ power law found in graphene [16], which has nodal points instead of nodal lines, and the even slower $\sim 1/\sqrt[3]{t}$ power law found in Weyl nodes [21]. Figure 3(b) shows an example of the low-density relaxation in a NLSM (brown curve). The exponential dependence is more evident in the log plot inset.

B. High-density limit

In this limit, we can use Eqs. (24), (25), and (31) to obtain

$$\frac{d}{dt}(k_B T_e) = -\gamma_{ad} \frac{1}{T_e}(T_e - T_L), \quad (33)$$

where $\gamma_{ad} = 3D^2 Q^3 \epsilon_F / 4\pi^2 \rho \hbar v^2$. We find linear relaxation for $T_e \gg T_L$ with a relaxation *rate* that scales as $\gamma_{ad} \sim n^{1/2}$ with electron density. This is different from graphene, where the relaxation rate scales as $\sim n^{3/2}$ [16]. Finally, the relaxation is exponential for $T_e \gtrsim T_L$ with timescale T_L/γ_{ad}.

Figure 3(b) shows the temperature relaxation in the high-density regime of a NLSM (orange or blue curve). The appearance of a linear relaxation in the temperature range $T_1^* > T > T_2^*$ is evident and is in agreement with Eq. (33). T_1^* is the crossover temperature between optical relaxation and acoustic relaxation (see Sec. V). T_2^* marks the regime transition from linear to exponential relaxation. There is an exponential relaxation for $T < T_2^*$.

V. CROSSOVER TEMPERATURE

The temperature T_1^* at which

$$\mathcal{P}_a(T_1^*) = \mathcal{P}_o(T_1^*) \quad (34)$$

defines the boundary between the regime dominated by optical phonons ($> T_1^*$) and the regime dominated by acoustic phonons ($< T_1^*$). If the initial temperature is $T_0 > T_1^*$, the decay is initially fast, followed by a slower decay. If $T_0 < T_1^*$, the decay is slower, and the electron plasma is longer lived.
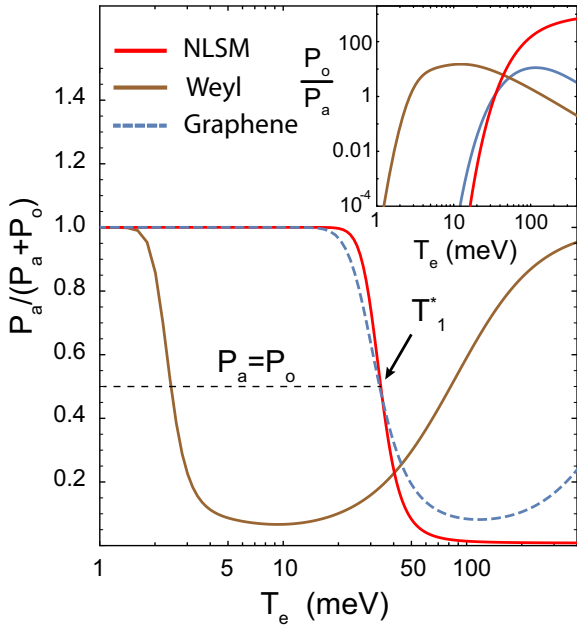
FIG. 5. Percentage of acoustic phonon cooling power as a function of electron temperatures for a NLSM, graphene, and a Weyl SM. Parameters are given in Table III.

Hence, an estimate of the crossover temperature is important for experimental design, device design, and as a control knob in probing microscopic mechanisms in materials. We consider two limiting cases in detail.

A. Low-density limit

Case 1: $\hbar\omega_0 \gg k_B T_e \gg k_B T_L, \mu$. From Eqs. (10), (15), and (31) we find that $\bar{\beta}^* = \hbar\omega_0/k_B T_1^*$ satisfies

$$\alpha_1 \equiv \frac{\pi^2 D^2 Q^2 \hbar}{2\rho g^2 \omega_0} = [(\bar{\beta}^*)^3 + 36\zeta(3)]e^{-\bar{\beta}^*}. \quad (35)$$

The left-hand side is a constant that depends on materials' properties. The right-hand side depends on $\bar{\beta}^*$. The intersection of the two gives the solution. Note that if $\alpha_1 < 36\zeta(3)$ and $\bar{\beta}^* \gg 1$, there is a solution.

Case 2: $k_B T_e \gg \hbar\omega_0, k_B T_L, \mu$. From Eqs. (10), (21), and (31), we find that $\bar{\beta}^* = \hbar\omega_0/k_B T_1^*$ satisfies

$$\alpha_1 = 2\pi^2 - \bar{\beta}^{*2} + \frac{\bar{\beta}^{*3}}{2} + \cdots. \quad (36)$$

There is a solution when $\alpha_1 < 2\pi^2$ and $\bar{\beta}^* \ll 1$.

B. High-density limit

Case 1: $\mu, \hbar\omega_0 \gg k_B T_e \gg k_B T_L$. From Eqs. (10), (23), and (31), we find that $\bar{\beta}^* = \hbar\omega_0/k_B T_1^*$ satisfies

$$\alpha_2 \equiv \frac{3 D^2 Q^2 \mu^2}{2\rho g^2 \omega_0^3 \hbar} = \left[\bar{\beta}^*(1 + 4\bar{\mu}^3) + 4\pi^2 \frac{\bar{\mu}}{\bar{\beta}^*} \right] e^{-\bar{\beta}^*}. \quad (37)$$

Using the parameters in Table III, $\alpha_2 = 0.0042$, and the intersection with the term on the right is at $k_B T_1^* = \hbar\omega_0/\bar{\beta}^* = 34$ meV, which is close to the full numerical solution $k_B T_1^* = 35$ meV shown in Fig. 5.

TABLE III. Parameters of a prototypical NLSM from Ref. [41], a Weyl SM, and doped graphene. The electron-phonon coupling constants for NLSMs are unknown. For a Weyl SM, we take the known parameters of TaAs [10].

	NLSM	Weyl	Graphene
ρ (kg/m^3, kg/m^2)	4.86	12.03	3.7×10^{-7}
n (cm^{-3}, cm^{-2})	5×10^{19}	10^{14}	10^{13}
ϵ_F (meV)	300	6	370
Q (1/Å)	0.3		
$\hbar\omega_0$ (meV)	300	31	196
D (eV)	5	4	20
v (10^6 m/s)	1	0.5	1
a (Å)	4	6.3	1.42
g ($v\hbar^2/a^2\sqrt{\rho\hbar\omega_0}$)	56.6	4.2	1.4
T_L (meV)	1	1	1

Case 2: $\mu \gg k_B T_e \gg \hbar\omega_0, k_B T_L$. From Eqs. (10), (23), and (31) and $N_e - N_L \sim 1/\bar{\beta}$, we find

$$k_B T_1^* = \frac{DQ\hbar}{2\pi g}\left(\frac{3\mu}{2\rho}\right)^{1/2} \sim n^{1/4}. \quad (38)$$

VI. ACOUSTIC AND OPTICAL PHONON RELAXATION: NUMERICAL SOLUTION

In this section, we solve numerically for $T_e(t)$ and $\mu(t)$ in the presence of acoustic and optical phonons. The basic equations are

$$\frac{d\mathcal{E}}{dt} = -\mathcal{P}_a - \mathcal{P}_o, \quad (39)$$

$$n = \frac{1}{V}\sum_{n\mathbf{k}} f_{n\mathbf{k}}. \quad (40)$$

The first equation gives the energy dynamics, and the second gives the constant electron density condition. $\mathcal{P}_a$ and $\mathcal{P}_o$ are the acoustic and optical phonon cooling power in Eqs. (10) and (31), and $\mathcal{E}$ is the energy,

$$\mathcal{E} = \frac{1}{V}\sum_{n\mathbf{k}} \epsilon_{n\mathbf{k}} f_{n\mathbf{k}}. \quad (41)$$

More explicitly, Eq. (39) becomes

$$-3QT_e v\hbar\left(\frac{\partial}{\partial t}\frac{1}{T_e}\right)I_{2+} + 2QT_e\left(\frac{\partial}{\partial t}\frac{\mu}{T_e}\right)I_{1-}$$
$$= -\frac{D^2 Q^4 k_B}{4\pi\rho v^2 \hbar}I_{1+}(T_e - T_L) - \frac{g^2 Q^2 \omega_0^4}{2\pi v^4 \hbar}F(N_e - N_L), \quad (42)$$

and the constant-density condition

$$n = \frac{Q}{2\pi}I_{1-}. \quad (43)$$

The initial conditions are $\mu(t=0) = \mu_0$, which is given by the electron density and $T_e(t=0) = T_0$. Figure 3 shows the electron temperature as a function of time for a NLSM with parameters given in Table III. The initial temperature is $T_0 = 100$ meV $= 1200$ K. Note the sharp change in behavior at temperature T_1^*. For $T_e > T_1^* \sim 35$ meV, there is a fast relaxation associated with optical phonons. At these temperatures,

$\mathcal{P}_a \ll \mathcal{P}_o$ (see Fig. 5). For $T_e < T_1^*$, acoustic phonons saturate the cooling power and dominate the relaxation process. In the optical phonon regime, the relaxation timescale is picoseconds, but in the acoustic phonon regime, the relaxation timescale is nanoseconds. As expected, the optical phonon relaxation is faster than acoustic phonon relaxation [1].

Note that the higher the density is, the faster the relaxation is. In the optical phonon regime at any density, the relaxation is of the inverse log form, as indicated in Eq. (20) or Eq. (27), even though $\bar{\beta}_0$ is only 3. In the acoustic phonon, low-density regime, the relaxation is exponential for $T_e < T_1^*$ [brown curve; Eq. (32)] and linear-exponential (orange curve) in the high-density regime [Eq. (33)]. The relaxation timescale depends weakly on density in the optical phonon regime and strongly in the acoustic phonon regime. Although not shown, the chemical potential increases monotonically towards ϵ_F as time increases.

In the optical phonon regime, $\mathcal{P}_a$ is expected to be low. What is interesting is that $\mathcal{P}_a$ in NLSMs is lower than in Weyl SMs and graphene (see Fig. 5). In fact, in NLSMs, there is a clean separation of scattering processes at T_1^*, which justifies considering optical and phonon scattering separately in Secs. III and IV.

Figure 4 shows the relaxation of a NLSM in the regime $k_B T_e \gg \hbar\omega_0$. Since emission of optical phonons is readily available, we expect a faster relaxation, as shown.

VII. ACOUSTIC PHONON RELAXATION IN DIRAC MATERIALS

The role of the nodal line is most critical in the acoustic phonon, low-density regime. This is expected because at low density ($\mu = 0$) acoustic phonons probe quasiparticles near the nodal line in NLSMs or nodal points in Weyl SMs or graphene. In this regime, the NLSM has exponential relaxation, Weyl SMs have $\sim 1/\sqrt[3]{t}$ relaxation, and graphene has $\sim 1/\sqrt[2]{t}$. To understand this, we write the energy relaxation equation as $\mathcal{C}dT_e/dt = -\mathcal{P}_a$, where the heat capacity $\mathcal{C} = d\mathcal{E}(\mu(T_e), T_e)/dT_e$. By power counting, we can write

$$\frac{dT_e}{dt} \sim -T_e^\kappa (T_e - T_L), \tag{44}$$

with $\kappa = \dim(\mathcal{P}_a - 1) - \dim\mathcal{C}$ or

$$\kappa = \{2(\mathcal{D} - d) - 1 + 2[q] - 1\} - (\mathcal{D} - d + a - 1). \tag{45}$$

To obtain $\dim\mathcal{C}$, we can inspect Eq. (12). We first subtract d nodal (frozen) directions from $\mathcal{D}$ spatial dimensions and add the power of the quasiparticle dispersion k^a (1 in this case). The temperature derivative of the energy gives the last -1. The electronic heat capacity scales as T_e with a power of 3 in Weyl nodes and with a power of 2 in graphene and NLSMs. In this sense, NLSMs and graphene are similar.

To obtain $\dim\mathcal{P}_a - 1$, we can inspect Eq. (8). We have $2(\mathcal{D} - d)$ powers from the integrals, subtract 1 from the energy conservation, and add 2 if momentum transfer $[q]$ is not constrained, i.e., in Weyl nodes and graphene. Finally, we subtract 1 from the Fermi function differences. The last two steps occur because we expanded the integrals to lowest order in c/v. The role of the nodal line is now explicit. From Eq. (45), $\dim\mathcal{P}_a - 1 = 6$ for Weyl SMs, $\dim\mathcal{P}_a - 1 = 4$ for graphene,

TABLE IV. Cooling power and heat capacity scaling with temperature for Dirac materials (see Sec. VIII). $\mathcal{D}$ is the spatial dimension, d is the nodal manifold dimension, $\dim\mathcal{C}$ is the scale dimension of the heat capacity, and $\dim\mathcal{P}_a$ is the scale dimension of acoustic phonon cooling power.

	NLSM	Weyl	Graphene
$\mathcal{D}$	3	3	2
d	1	0	0
$2[q]$	0	2	2
$\dim\mathcal{C}$	2	3	2
$\dim\mathcal{P}_a - 1$	2	6	4
κ	0^a	3^b	2^c

[a]Equation (32).
[b]Equation (D19).
[c]Equation (E5).

and $\dim\mathcal{P}_a - 1 = 2$ for NLSMs (see Table IV). It is lowest in NLSMs. There are two consequences: (a) a large decrease in $\mathcal{P}_a$ in a NLSM at high temperature compared with Weyl SMs and graphene (see Fig. 5), and (b) at low temperatures, it gives the exponential temperature relaxation in NLSMs and a slower power law in graphene and Weyl SMs.

VIII. DISCUSSION AND CONCLUSIONS

We calculated the electron temperature relaxation as a function of time after a sudden excitation. We used a two-band model of a NLSM with a single acoustic branch and a single optical branch. Among our findings, we point out that acoustic phonon relaxation is exponential, which is similar to standard 3D metals [3] but different from Weyl SMs and graphene. This is because a particular combination of FS volume and topology in NLSMs. Other relaxation behaviors were obtained depending on initial conditions and density and were summarized in Table II. Our results point to possible ways to engineer thermalization timescales, e.g., by tuning either density, spatial dimension, or the shape of the FS.

We assumed that phonons of large momenta $\sim 2Q$ can be thermally excited, and this puts a lower bound on T_e, $k_B T_e > \hbar c 2Q \equiv k_B T_{BG}$. For ZrSiS [41] with $c = 4.3$–6.8 km/s and $Q \sim 0.3$ Å^{-1} we obtain $k_B T_{BG} = 17$–26 meV $= 197$–300 K. For PbTaSe$_2$ [26,42] with roughly the same sound speed and half of the Q we obtain $k_B T_{BG} = 98 - 150$ K.

We have assumed particle-hole symmetry, time reversal symmetry, and a highly symmetric nodal line. Our conclusions will not change for small deviations of these symmetries. If there is more than one ring or if we consider the spin of the electrons, the total cooling power is multiplied by the number of equivalent rings and by the spin degeneracy, but $T_e(t)$ will not change. In this work we assumed a clean system; future work is needed to understand impurity effects.

APPENDIX A: PHONON COOLING POWER

From Eqs. (4), (5), and (6) we obtain

$$\mathcal{P} = \frac{1}{V} \sum_{n\mathbf{k}} \sum_{m\mathbf{p}} (\epsilon_{n\mathbf{k}} - \epsilon_{m\mathbf{p}}) f_{n\mathbf{k}} (1 - f_{m\mathbf{p}}) W_{n\mathbf{k},m\mathbf{p}} \quad \text{(A1)}$$

$$= \mathcal{P}_1 + \mathcal{P}_2, \quad \text{(A2)}$$

where

$$\mathcal{P}_1 = \frac{2\pi}{\hbar} \frac{1}{V} \sum_{n\mathbf{k}} \sum_{m\mathbf{p}} (\epsilon_{n\mathbf{k}} - \epsilon_{m\mathbf{p}})(f_{n\mathbf{k}} - f_{m\mathbf{p}}) M_\mathbf{q} N_L$$

$$\times \delta(\epsilon_{n\mathbf{k}} - \epsilon_{m\mathbf{p}} - \hbar\omega_\mathbf{q}), \quad \text{(A3)}$$

$$\mathcal{P}_2 = \frac{2\pi}{\hbar} \frac{1}{V} \sum_{n\mathbf{k}} \sum_{m\mathbf{p}} (\epsilon_{n\mathbf{k}} - \epsilon_{m\mathbf{p}}) f_{n\mathbf{k}} (1 - f_{m\mathbf{p}}) M_\mathbf{q}$$

$$\times \delta(\epsilon_{n\mathbf{k}} - \epsilon_{m\mathbf{p}} - \hbar\omega_\mathbf{q}). \quad \text{(A4)}$$

In obtaining Eqs. (A3) and (A4), we assumed $\omega_{-\mathbf{q}} = \omega_\mathbf{q}$, which holds for time reversal symmetric systems or inversion symmetric systems. Using the identity

$$f_{n\mathbf{k}}(1 - f_{m\mathbf{p}}) \delta(\epsilon_{n\mathbf{k}} - \epsilon_{m\mathbf{p}} - \hbar\omega_\mathbf{q})$$

$$= -(f_{n\mathbf{k}} - f_{m\mathbf{p}}) N_e(\hbar\omega_\mathbf{q}) \delta(\epsilon_{n\mathbf{k}} - \epsilon_{m\mathbf{p}} - \hbar\omega_\mathbf{q}), \quad \text{(A5)}$$

$\mathcal{P}_2$ becomes

$$\mathcal{P}_2 = -\frac{2\pi}{\hbar} \frac{1}{V} \sum_{n\mathbf{k}} \sum_{m\mathbf{p}} (\epsilon_{n\mathbf{k}} - \epsilon_{m\mathbf{p}})(f_{n\mathbf{k}} - f_{m\mathbf{p}}) M_\mathbf{q} N_e$$

$$\times \delta(\epsilon_{n\mathbf{k}} - \epsilon_{m\mathbf{p}} - \hbar\omega_\mathbf{q})$$

$$\equiv -\mathcal{P}_1(L \to e). \quad \text{(A6)}$$

This relation (noted in Ref. [17]) means Eq. (4) in the main text becomes

$$\mathcal{P} = \frac{2\pi}{V\hbar} \sum_{n\mathbf{k}m\mathbf{p}} (\epsilon_{n\mathbf{k}} - \epsilon_{m\mathbf{p}})(f_{n\mathbf{k}} - f_{m\mathbf{p}})(N_L - N_e) M_\mathbf{q}$$

$$\times \delta(\epsilon_{n\mathbf{k}} - \epsilon_{m\mathbf{p}} - \hbar\omega_\mathbf{q}), \quad \text{(A7)}$$

which is Eq. (8) in the main text.

APPENDIX B: OPTICAL PHONON COOLING IN NLSMs

We start from Eqs. (A3) and set $M_\mathbf{q} = g^2/V$, $\omega_\mathbf{q} = \omega_0$ to obtain

$$\mathcal{P}_{o1} = 2\pi g^2 N_L \omega_0 \frac{1}{V^2} \sum_{n\mathbf{k}} \sum_{m\mathbf{p}} (f_{n\mathbf{k}} - f_{n\mathbf{p}}) \delta(\epsilon_{n\mathbf{k}} - \epsilon_{n\mathbf{p}} - \hbar\omega_0). \quad \text{(B1)}$$

Now, we write the sums over momenta as integrals in cylindrical coordinates. Then we define a new variable $k' \equiv k - Q$. The integral over k' is now from $-Q$ to ∞. Next, we extend the integration of k' to the whole real line and parametrize the

plane k'-k_z in polar coordinates $\tilde{k}, \phi_{\tilde{k}}$ to obtain

$$\mathcal{P}_{o1} = g^2 N_L \omega_0 \frac{1}{(2\pi)^3} \sum_{nm} \int \tilde{k} d\tilde{k} d\phi_{\tilde{k}} \int \tilde{p} d\tilde{p} d\phi_{\tilde{p}}$$

$$\times (\tilde{k}\sin\phi_{\tilde{k}} + Q)(\tilde{p}\sin\phi_{\tilde{p}} + Q)[f(nv\hbar\tilde{k}) - f(mv\hbar\tilde{p})]$$

$$\times \delta(\epsilon_{n\tilde{k}} - \epsilon_{n\tilde{p}} - \hbar\omega_0) \quad \text{(B2)}$$

$$= g^2 N_L \omega_0 \frac{Q^2}{2\pi v\hbar} \sum_{nm} \int \tilde{k} d\tilde{k} \int \tilde{p} d\tilde{p}$$

$$\times \left[f(nv\hbar\tilde{k}) - f(mv\hbar\tilde{p})\right] \delta(n\tilde{k} - m\tilde{p} - \omega_0/v), \quad \text{(B3)}$$

where in the last equality we use the fact that the δ function fixes $m\tilde{p} = n\tilde{k} + \omega_0/v$ and that the Fermi function difference is very small for $\tilde{k} \gg \omega_0/v$. This justifies extending the limits of integrals to the whole real line as long as $Q \gg \omega_0/v, k_B T_e/v\hbar$. After some algebra

$$\mathcal{P}_{o1} = -\frac{g^2 \omega_0^4 Q^2}{2\pi v^4 \hbar} F N_L, \quad \text{(B4)}$$

where F is given by Eq. (11). Finally, $\mathcal{P}_o = \mathcal{P}_{o1}(L) - \mathcal{P}_{o1}(L \to e)$ gives Eq. (10) in the main text.

APPENDIX C: ACOUSTIC PHONON COOLING IN NLSMs

Starting from Eq. (A3), we substitute $M_\mathbf{q}$, $\omega_\mathbf{q} = cq = c|\mathbf{k} - \mathbf{p}|$ and assume the lattice temperature is such that $k_B T_L \gg \hbar\omega_\mathbf{q}$. This requires $T_L > T_{BG}$, as discussed in the main text. We obtain

$$\mathcal{P}_{a1} = \frac{2\pi D^2 k_B T_L}{4\rho V^2 c^2} \sum_{n\mathbf{k}} \sum_{m\mathbf{p}} \omega_\mathbf{q} (f_{n\mathbf{k}} - f_{m\mathbf{p}})$$

$$\times (1 + s_{nm} \cos\theta) \delta(\epsilon_{n\mathbf{k}} - \epsilon_{m\mathbf{p}} - \hbar\omega_\mathbf{q}). \quad \text{(C1)}$$

Now, we write the sums over momenta as integrals in cylindrical coordinates and define $k' = k - Q$. The integral over k' is now from $-Q$ to ∞. The Fermi functions limit the size of k' to values near $|k_F - Q| \ll Q$. Hence, we can extend the limits of integration of the radial component k' to the whole real line with small error as long as $Q \gg |k_F - Q|, k_B T_e$. Now we transform the k' and k_z variables to polar coordinates $\tilde{k}, \phi_{\tilde{k}}$. In terms of these variables, $k' = \tilde{k}\sin\phi_{\tilde{k}}, k_z = \tilde{k}\cos\phi_{\tilde{k}}$, and the dispersion relation $\epsilon_{n\mathbf{k}}$ is that of a Dirac cone in two dimensions. The energy difference becomes $\epsilon_{n\mathbf{k}} - \epsilon_{m\mathbf{p}} = v\hbar(n\tilde{k} - m\tilde{p})$, and the delta function

$$\delta(\epsilon_{n\mathbf{k}} - \epsilon_{m\mathbf{p}} - \hbar\omega_\mathbf{q}) = \frac{1}{v\hbar} \delta(n\tilde{k} - m\tilde{p} - rq) \quad \text{(C2)}$$

$$= \frac{1}{v\hbar} \delta_{nm} \delta(\tilde{p} - \tilde{p}_0)[1 + O(r)], \quad \text{(C3)}$$

fixes $\tilde{p}$ to $\tilde{p}_0 = \tilde{k} - nr[q]_{\tilde{p}=\tilde{k}}$ (to first order in $r \equiv c/v$). $[q]_{\tilde{p}=\tilde{k}}$ is the phonon momentum to zeroth order, i.e., equal to $q = |\mathbf{k} - \mathbf{p}|$ with $\tilde{p} = \tilde{k}$. In the limit $Q \gg \tilde{k}_F$

$$q^2 \approx 2Q^2(1 - \cos\phi), \quad \text{(C4)}$$

$$1 + s_{nm} \cos\theta \approx 1 + s_{nm} \cos\phi, \quad \text{(C5)}$$

where $\phi \equiv \phi_\mathbf{k} - \phi_\mathbf{p}$. This means that the phonon momentum is effectively 2D in the plane k_x-k_y. Finally, we note $\hbar\omega_\mathbf{q}$ and

the Fermi function difference are both $O(r)$, and hence, we can set $\tilde{p} = \tilde{k}$ in the rest of the factors of Eq. (C1). Note that

$$f_{n\tilde{k}} - f_{n\tilde{p}} = nr\tilde{q} \frac{\partial f_{n\tilde{k}}}{\partial \tilde{k}} + O(r^2) \qquad (C6)$$

is peaked at $\tilde{k} \sim \tilde{k}_F$. As a result Eq. (C1) becomes

$$\mathcal{P}_{a1} = -\frac{D^2 Q^4 k_B}{4\pi \rho v^2 \hbar} I_{1,+} T_L, \qquad (C7)$$

where

$$I_{n\pm} \equiv \int_0^\infty \tilde{k}^n d\tilde{k} [f_{c\tilde{k}} \pm (1 - f_{v\tilde{k}})], \qquad (C8)$$

and $f_{n\tilde{k}} = [e^{(nv\hbar\tilde{k} - \mu)\beta} + 1]^{-1}$.

APPENDIX D: PHONON COOLING POWER IN A WEYL NODE

The quasiparticle energy near a Weyl node is $\epsilon_{n\mathbf{k}} = nv\hbar k$, where $k = |\mathbf{k}|$ is the magnitude of a 3D momentum and $n = \pm 1$ denote the conduction ($+1$) and valence (-1) bands. The FS is a sphere in momentum space.

1. Optical phonon relaxation

Following the steps outlined in Appendix B, the cooling power of optical phonons in a Weyl node is

$$\mathcal{P}_{wo} = \frac{\omega_0^6 g^2}{v^6 \hbar 2\pi^3} H(N_e - N_L), \qquad (D1)$$

where

$$H \equiv \int_{-\infty}^\infty dx\, x^2 (x-1)^2 [f(\hbar\omega_0 x - \hbar\omega_0) - f(\hbar\omega_0 x)]$$
$$= \frac{1}{30} + \bar{\mu}^4 + \frac{2\pi^2 \bar{\mu}^2}{\bar{\beta}^2} + \frac{7\pi^4}{15\bar{\beta}^4}, \qquad (D2)$$

has a simple closed form valid in all regimes of $\bar{\beta} \equiv \hbar\omega_0 / k_B T_e$ and $\bar{\mu} \equiv \mu / \hbar\omega_0$.

a. Low-density limit

Case 1: $\hbar\omega_0 \gg k_B T_e \gg T_L, \mu$. If $\bar{\beta} \gg 1$ and $T_e \gg T_L$, then $N_e - N_L \sim e^{-\bar{\beta}}$. The energy and density,

$$\mathcal{E} = \frac{v\hbar I_{3+}}{2\pi^2} = \frac{k_B^4 T_e^4 7\pi^2}{120 v^3 \hbar^3} + \frac{k_B^2 T_e^2 \mu^2}{4 v^3 \hbar^3} + \cdots \quad \mu \ll k_B T_e, \quad (D3)$$

$$n = \frac{I_{2-}}{2\pi^2} = \frac{k_B^3 T_e^3 \mu}{6 v^3 \hbar^3} + \cdots \quad \mu \ll k_B T_e, \qquad (D4)$$

together with Eq. (D2) and $d\mathcal{E}/dt = -\mathcal{P}_{wo}$ give

$$\frac{d\bar{\beta}}{dt} = \tilde{\gamma}_{won1}(\bar{\beta}^5 + 14\pi^4 \bar{\beta}) e^{-\bar{\beta}}. \qquad (D5)$$

To leading order as $\bar{\beta} \gg 1$, the relaxation is an inverse log,

$$k_B T_e = \frac{\hbar\omega_0}{\log(\gamma_{won1} \bar{\beta}_0^5 t + e^{\bar{\beta}_0})}, \qquad (D6)$$

where $\bar{\beta}_0 \equiv \hbar\omega_0 / k_B T_0 \gg 1$, $\gamma_{won1} = g^2 \omega_0^2 / 14\pi^5 v^3 \hbar^2$, and the relaxation timescale is $e^{\bar{\beta}_0} / \gamma_{won1} \bar{\beta}_0^5$.

Case 2: $k_B T_e \gg \hbar\omega_0, T_L, \mu$. In this limit, $N_e - N_L \sim 1/\bar{\beta}$, and hence, to leading order

$$k_B T_e = \frac{\hbar\omega_0}{\gamma_{won2} t + \bar{\beta}_0}, \qquad (D7)$$

where $\gamma_{won2} = g^2 \omega_0^2 / \pi^3 v^3 \hbar^2$.

b. High-density limit

Case 1: $\mu, \hbar\omega_0 \gg k_B T_e \gg T_L$. In the limit of a large chemical potential $\mu \gg k_B T_e$ the energy and density are

$$\mathcal{E} = \frac{1}{8\pi^2 v^3 \hbar^3} \left(\mu^4 + \frac{2\pi^2 \mu^2}{\beta^2} + \cdots \right), \quad \mu \gg k_B T_e, \quad (D8)$$

$$n = \frac{1}{6\pi^2 v^3 \hbar^3} \left(\mu^3 + \frac{\pi^2 \mu}{\beta^2} + \cdots \right), \quad \mu \gg k_B T_e. \quad (D9)$$

The last equation implies $\mu(T_e) = \epsilon_F - \pi^2 k_B^2 T_e^2 / 3\epsilon_F + \cdots$ and together with $N_e - N_L \sim e^{-\bar{\beta}}$ and Eq. (D2) gives

$$\frac{\partial \bar{\beta}}{\partial t} = \tilde{\gamma}_{wod1} \bar{\beta}^3 \left(\frac{1}{30} + \bar{\mu}^4 + \frac{2\pi^2 \bar{\mu}^2}{\bar{\beta}^2} + \frac{7\pi^4}{15\bar{\beta}^4} \right) e^{-\bar{\beta}}. \quad (D10)$$

If $\bar{\mu}\bar{\beta} \gg \pi\sqrt{2}$, the leading behavior is given by the first two terms on the right, and we obtain

$$k_B T_e = \frac{\hbar\omega_0}{\log(\gamma_{wod1} \bar{\beta}_0^3 t + e^{\bar{\beta}_0})}, \qquad (D11)$$

with $\gamma_{wod1} = 3g^2 \omega_0^4 (1/30 + \bar{\mu}^4) / \pi^2 v^3 \mu^2$ and timescale $e^{\bar{\beta}_0} / \gamma_{wod1} \bar{\beta}_0^3$. The timescale is $\sim n^{2/3}$ for $\bar{\mu} \ll 1$ and $\sim n^{-2/3}$ for $\bar{\mu} \gg 1$.

Case 2: $\mu \gg k_B T_e \gg \hbar\omega_0, T_L$. In this case $N_e - N_L \sim 1/\bar{\beta}$, and from Eqs. (D2), (D8), and (D9) we obtain

$$\frac{d\bar{\beta}}{dt} = \tilde{\gamma}_{wod2} \bar{\beta}^2 \left(\frac{1}{30} + \bar{\mu}^4 + \frac{2\pi^2 \bar{\mu}^2}{\bar{\beta}^2} + \frac{7\pi^4}{15\bar{\beta}^4} \right). \quad (D12)$$

If $\bar{\mu}\bar{\beta} \gg \pi\sqrt{2}$, the leading behavior is

$$\frac{d\bar{\beta}}{dt} = \gamma_{wod2} \bar{\beta}^2 \qquad (D13)$$

or

$$k_B T_e = k_B T_0 - \hbar\omega_0 \gamma_{wod2} t, \qquad (D14)$$

where the relaxation rate $\gamma_{wod2} = 3g^2 \omega_0^4 (1/30 + \bar{\mu}^4) / \pi^2 v^3 \mu^2$ scales as $\sim n^{-2/3}$ for $\bar{\mu} \ll 1$ and as $\sim n^{2/3}$ for $\bar{\mu} \gg 1$.

2. Acoustic phonon relaxation

The cooling power of acoustic phonons in a Weyl SM was studied in Ref. [21]. Here, we reproduce those results for comparison. Following the same steps as in Appendix C, we obtain

$$\mathcal{P}_{wa1} = -\frac{D^2 k_B}{\hbar \rho v^2 \pi^3} I_{5+} T_L, \qquad (D15)$$

and hence, the cooling power of acoustic phonons is [21]

$$\mathcal{P}_{wa} = \mathcal{P}_{wa1}(L) - \mathcal{P}_{wa1}(L \to e) = \frac{D^2 k_B}{\rho v^2 \hbar \pi^3} I_{5+}(T_e - T_L), \quad (D16)$$

where

$$I_{n\pm} \equiv \int_0^\infty k^n dk \, [f_{ck} \pm (1 - f_{vk})], \tag{D17}$$

and $f_{nk} = [e^{\beta(nv\hbar k - \mu)} + 1]^{-1}$.

a. Low-density limit

If $\mu = 0$, we can integrate (D16) analytically to obtain

$$\mathcal{P}_{wa} = \frac{D^2 k_B^7 T_e^6 31\pi^3}{\rho v^8 \hbar^7 126}(T_e - T_L). \tag{D18}$$

The energy and density of a Weyl node are given by Eqs. (D3) and (D4), and with $d\mathcal{E}/dt = -\mathcal{P}_{wa}$ we obtain

$$\frac{dT_e}{dt} = -\gamma_{wan} T_e^3 (T_e - T_L), \tag{D19}$$

where $\gamma_{wan} = 155\pi D^2 k_B^3 / 147\rho v^5 \hbar^4$. If $T_e \gg T_L$, T_e relaxes as a power law [21],

$$T_e = \frac{T_0}{(1 + 3\gamma_{wan} T_0^3 t)^{1/3}}, \tag{D20}$$

with timescale $1/3\gamma_{wan}T_0^3$, but if $T_e \gtrsim T_L$, T_e relaxes exponentially with timescale $1/\gamma_{wan}T_L^3$.

b. High-density limit

Using Eqs. (D8), (D9), and (D16), we have to leading order [21]

$$\frac{d}{dt}k_B T_e \sim -\gamma_{wad}\frac{1}{T_e}(T_e - T_L), \tag{D21}$$

where $\gamma_{wad} = D^2 \mu^4 / 3\pi^3 \rho v^5 \hbar^4$. So for $T_e \gg T_L$ the relaxation is linear,

$$k_B T_e \sim k_B T_0 - \gamma_{wad} t, \tag{D22}$$

with a rate that scales as $\sim n^{4/3}$ with the electron density. In the limit $T_e \gtrsim T_L$, the relaxation is exponential with timescale $T_L/\gamma_{wad} \sim n^{-4/3}$.

APPENDIX E: PHONON COOLING POWER IN GRAPHENE

In this Appendix, we calculate the temperature relaxation in graphene due to acoustic and optical phonons. The dispersion relation of quasiparticles near a nodal point is $\epsilon_{n\mathbf{k}} = nv\hbar k$, where $k = |\mathbf{k}|$ is a 2D wave vector.

1. Optical phonon relaxation

Following the same steps as in Appendix B and using $\omega_{\mathbf{q}} = \omega_0$ and $M_{\mathbf{q}} = g^2/V$, we obtain [16]

$$\mathcal{P}_{go} = \frac{g^2 \omega_0^4}{2\pi v^4 \hbar} F(\mu, T_e)(N_e - N_L), \tag{E1}$$

where F is given in Eq. (11) and Eqs. (15) and (21) are valid for graphene too.

a. Low-density limit

Case 1: $\hbar\omega_0 \gg k_B T_e \gg T_L, \mu$. The energy and particle density, $\mathcal{E} = v\hbar I_{2+}/2\pi$ and $n = I_{1-}/2\pi$, are the same as for NLSMs [Eqs. (16) and (17)] except for a trivial factor of Q, which is absent in graphene. Defining as before $\bar{\beta} \equiv \hbar\omega_0/k_B T_e$ and using (E1), we find

$$\frac{\partial\bar{\beta}}{\partial t} = \gamma_{gon1}(\bar{\beta}^4 + 36\zeta(3)\bar{\beta} + \cdots)e^{-\bar{\beta}}, \tag{E2}$$

where $\gamma_{gon1} = g^2\omega_0/54\zeta(3)v^2\hbar^2$ and to leading order in $\bar{\beta} \gg 1$ we obtain an inverse log form,

$$k_B T_e = \frac{\hbar\omega_0}{\log(\gamma_{gon1}\bar{\beta}_0^4 t + e^{\bar{\beta}_0})}. \tag{E3}$$

Case 2: $k_B T_e \gg \hbar\omega_0, k_B T_L, \mu$. In the opposite regime where $k_B T_e \gg \hbar\omega_0$ the same considerations apply as in NLSMs, and we obtain an exponential relaxation [see Eq. (22)], but the factor of Q is absent in graphene.

b. High-density limit

The considerations in Sec. III B apply for graphene as well. We obtain the same relaxation forms as in Eqs. (27) and (29), but the factor of Q is absent in graphene.

2. Acoustic phonon relaxation

The temperature relaxations due to acoustic phonon scattering in NLSMs and graphene are different because the nodal line affects NLSMs in a nontrivial way (see Appendix C). The temperature relaxation in graphene due to acoustic phonons was presented by Bistritzer and MacDonald [16] and is included here for comparison with NLSMs. From Eq. (8) we obtain

$$\mathcal{P}_{ga} = \frac{D^2 k_B}{\rho v^2 \hbar 2\pi} I_{3+}(T_e - T_L), \tag{E4}$$

where I_{3+} is given in Eq. (C8) and in closed form in Ref. [17].

a. Low-density limit

Equations (16) and (17) in the limit $\mu \ll k_B T_e$ are also valid for graphene if we omit the factor of Q. From the equation of motion $(\partial\mathcal{E}/\partial T_e)(\partial T_e/\partial t) = -\mathcal{P}_{ga}$ we obtain

$$\frac{dT_e}{dt} = -\gamma_{gan} T_e^2 (T_e - T_L), \tag{E5}$$

where $\gamma_{gan} = D^2 k_B^2 7\pi^4 / 540\zeta(3)\rho v^4 \hbar^3$. This means $T_e = T_0/(1 + t/\tau_{gan})^{1/2}$ for $T_e \gg T_L$. T_e is an exponential function with timescale $1/\gamma_{gan}T_L^2$ for $T_e \gtrsim T_L$.

b. High-density limit

Equations (24) and (25) are also valid for graphene after omitting the factor of Q, and we obtain

$$\frac{dT_e}{dt} = -\gamma_{gad}\frac{1}{T_e}(T_e - T_L), \tag{E6}$$

where $\gamma_{gad} = 3D^2 \mu^3 / 4\pi^2 k_B \rho v^4 \hbar^3$. This means the relaxation is linear for $T_e \gg T_L$, and the rate scales as $\sim n^{3/2}$ with electron density. The relaxation is exponential for $T_e \gtrsim T_L$.

[1] V. F. Gantmakher and Y. B. Levinson, *Carrier Scattering in Metals and Semiconductors* (Elsevier, New York, 1987).

[2] S. M. Sze, Y. Li, and K. K. Ng, *Physics of Semiconductor Devices*, 4th ed. (Wiley, Hoboken, NJ, 2021).

[3] P. B. Allen, Phys. Rev. Lett. **59**, 1460 (1987).

[4] F. C. Wellstood, C. Urbina, and J. Clarke, Phys. Rev. B **49**, 5942 (1994).

[5] M. Massicotte, G. Soavi, A. Principi, and K.-J. Tielrooij, Nanoscale **13**, 8376 (2021).

[6] A. Sergeev and V. Mitin, Phys. Rev. B **61**, 6041 (2000).

[7] J. T. Karvonen, L. J. Taskinen, and I. J. Maasilta, Phys. Rev. B **72**, 012302 (2005).

[8] F. W. J. Hekking, A. O. Niskanen, and J. P. Pekola, Phys. Rev. B **77**, 033401 (2008).

[9] S. S. Kubakaddi, Phys. Rev. B **79**, 075417 (2009).

[10] N. P. Armitage, E. J. Mele, and A. Vishwanath, Rev. Mod. Phys. **90**, 015001 (2018).

[11] H. L. Stormer, L. N. Pfeiffer, K. W. Baldwin, and K. W. West, Phys. Rev. B **41**, 1278 (1990).

[12] D. K. Efetov and P. Kim, Phys. Rev. Lett. **105**, 256805 (2010).

[13] W.-K. Tse and S. Das Sarma, Phys. Rev. B **79**, 235406 (2009).

[14] J. C. W. Song, M. Y. Reizer, and L. S. Levitov, Phys. Rev. Lett. **109**, 106602 (2012).

[15] M. W. Graham, S.-F. Shi, D. C. Ralph, J. Park, and P. L. McEuen, Nat. Phys. **9**, 103 (2013).

[16] R. Bistritzer and A. H. MacDonald, Phys. Rev. Lett. **102**, 206410 (2009).

[17] J. K. Viljas and T. T. Heikkilä, Phys. Rev. B **81**, 245404 (2010).

[18] Y. H. Wang, D. Hsieh, E. J. Sie, H. Steinberg, D. R. Gardner, Y. S. Lee, P. Jarillo-Herrero, and N. Gedik, Phys. Rev. Lett. **109**, 127401 (2012).

[19] J. Coulter, G. B. Osterhoudt, C. A. C. Garcia, Y. Wang, V. M. Plisson, B. Shen, N. Ni, K. S. Burch, and P. Narang, Phys. Rev. B **100**, 220301(R) (2019).

[20] G. B. Osterhoudt, Y. Wang, C. A. C. Garcia, V. M. Plisson, J. Gooth, C. Felser, P. Narang, and K. S. Burch, Phys. Rev. X **11**, 011017 (2021).

[21] R. Lundgren and G. A. Fiete, Phys. Rev. B **92**, 125139 (2015).

[22] A. A. Burkov, M. D. Hook, and L. Balents, Phys. Rev. B **84**, 235126 (2011).

[23] Y. Kim, B. J. Wieder, C. L. Kane, and A. M. Rappe, Phys. Rev. Lett. **115**, 036806 (2015).

[24] C. Fang, Y. Chen, H.-Y. Kee, and L. Fu, Phys. Rev. B **92**, 081201(R) (2015).

[25] C. Fang, H. Weng, X. Dai, and Z. Fang, Chin. Phys. B **25**, 117106 (2016).

[26] G. Bian, T.-R. Chang, R. Sankar, S.-Y. Xu, H. Zheng, T. Neupert, C.-K. Chiu, S.-M. Huang, G. Chang, I. Belopolski, D. S. Sanchez, M. Neupane, N. Alidoust, C. Liu, B. Wang, C.-C. Lee, H.-T. Jeng, C. Zhang, Z. Yuan, S. Jia, A. Bansil, F. Chou, H. Lin, and M. Z. Hasan, Nat. Commun. **7**, 10556 (2016).

[27] Y. Wu, L.-L. Wang, E. Mun, D. D. Johnson, D. Mou, L. Huang, Y. Lee, S. L. Bud'ko, P. C. Canfield, and A. Kaminski, Nat. Phys. **12**, 667 (2016).

[28] L. M. Schoop, M. N. Ali, C. Straßer, A. Topp, A. Varykhalov, D. Marchenko, V. Duppel, S. S. P. Parkin, B. V. Lotsch, and C. R. Ast, Nat. Commun. **7**, 11696 (2016).

[29] M. Neupane, I. Belopolski, M. M. Hosen, D. S. Sanchez, R. Sankar, M. Szlawska, S.-Y. Xu, K. Dimitri, N. Dhakal, P. Maldonado, P. M. Oppeneer, D. Kaczorowski, F. Chou, M. Z. Hasan, and T. Durakiewicz, Phys. Rev. B **93**, 201104(R) (2016).

[30] S.-Y. Yang, H. Yang, E. Derunova, S. S. P. Parkin, B. Yan, and M. N. Ali, Adv. Phys.: X **3**, 1414631 (2018).

[31] S. Klemenz, S. Lei, and L. M. Schoop, Annu. Rev. Mater. Res. **49**, 185 (2019).

[32] M. N. Ali, L. M. Schoop, C. Garg, J. M. Lippmann, E. Lara, B. Lotsch, and S. S. P. Parkin, Sci. Adv. **2**, e1601742 (2016).

[33] G. Gatti, A. Crepaldi, M. Puppin, N. Tancogne-Dejean, L. Xian, U. De Giovannini, S. Roth, S. Polishchuk, P. Bugnon, A. Magrez, H. Berger, F. Frassetto, L. Poletto, L. Moreschini, S. Moser, A. Bostwick, E. Rotenberg, A. Rubio, M. Chergui, and M. Grioni, Phys. Rev. Lett. **125**, 076401 (2020).

[34] Y. Shao, A. N. Rudenko, J. Hu, Z. Sun, Y. Zhu, S. Moon, A. J. Millis, S. Yuan, A. I. Lichtenstein, D. Smirnov, Z. Q. Mao, M. I. Katsnelson, and D. N. Basov, Nat. Phys. **16**, 636 (2020).

[35] S. T. Ramamurthy and T. L. Hughes, Phys. Rev. B **95**, 075138 (2017).

[36] A. N. Rudenko, E. A. Stepanov, A. I. Lichtenstein, and M. I. Katsnelson, Phys. Rev. Lett. **120**, 216401 (2018).

[37] Y. Huh, E.-G. Moon, and Y. B. Kim, Phys. Rev. B **93**, 035138 (2016).

[38] S. V. Syzranov and B. Skinner, Phys. Rev. B **96**, 161105(R) (2017).

[39] B. N. Narozhny and I. V. Gornyi, Front. Phys. **9**, 108 (2021).

[40] A. Lucas and K. C. Fong, J. Phys.: Condens. Matter **30**, 053001 (2018).

[41] A. N. Rudenko and S. Yuan, Phys. Rev. B **101**, 115127 (2020).

[42] T.-R. Chang, P.-J. Chen, G. Bian, S.-M. Huang, H. Zheng, T. Neupert, R. Sankar, S.-Y. Xu, I. Belopolski, G. Chang, B. K. Wang, F. Chou, A. Bansil, H.-T. Jeng, H. Lin, and M. Z. Hasan, Phys. Rev. B **93**, 245130 (2016).